MSEC2022-85673

NUMERICAL STUDIES ON COLD SPRAY PARTICLE DEPOSITION USING A RECTANGULAR NOZZLE

Ted Gabor[1], Semih Akin[1], Jung-Ting Tsai[2], Seunghwan Jo[1], Feraas Al-Najjar[1], Martin Byung-Guk Jun[1*]
[1] Purdue University, School of Mechanical Engineering, West Lafayette, IN, 47906, USA
[2] Purdue University, School of Materials Engineering, West Lafayette, IN, 47906, USA

ABSTRACT

Cold spray additive manufacturing (CSAM) is an emerging technique for scalable and rapid deposition of thick metallic coatings on various substrates. Despite great promises, CSAM with no upper limit of coating thickness remains challenging due to the stochastic nature of cold spray (CS) deposition. In particular, using axisymmetric nozzles (i.e., circular supersonic nozzles) lead to a quasi-Gaussian shaped particle distribution on the target surface, which limits the CSAM due to the formation of triangular-shaped (i.e., peak/valley-shaped) coating morphology. Recently, rectangular cold spray nozzles have been applied to CS particle deposition, and found to be promising for CSAM owing to its more uniform particle distribution and wider spray beam. In these studies, however, process-structure properties of cold spray deposition with a rectangular nozzle have not been sufficiently elucidated. Practical expansion of rectangular nozzles in CSAM strictly depends on uncovering process-structure properties of CS deposition phenomenon. To this end, we investigate cold spray deposition of microscale particles using a rectangular nozzle through three-dimensional discrete-phase turbulent flow modeling. The numerical modeling results are experimentally justified using a dual disc anemometer setup. The influence of operating gas conditions on critical particle deposition parameters is studied. An experimental case study of cold spray particle deposition on a polymer (ABS) substrate is also conducted to show the potential of rectangular nozzle in cold-spray based polymer metallization. The results suggest that cold spraying using a rectangular nozzle is beneficial for a more uniform, compact, and higher precision particle distribution on the target surface.

Keywords: Cold spray, numerical modeling, CFD, rectangular nozzle, additive manufacturing, polymer metallization

1. INTRODUCTION

Cold spray additive manufacturing (CSAM) is an emerging technique for one-step, scalable, and rapid deposition of thick metallic coatings on various substrates [1–3]. Cold spray (CS)

technology has grown substantially since the 1980's in a global manner [4]. The CS process involves feeding of metallic (e.g., aluminum and copper [3]) micro-scale powders into a converging-diverging (CD) nozzle (*i.e.*, supersonic nozzle), where the particles are accelerated high velocities (*e.g.*, 300-1200 m/s) using compressed gases such as helium, nitrogen, or argon [3]. Once the powders reach a critical velocity (that is dependent on the powder and substrate material), they have enough energy to imbed themselves onto a target surface through mechanical interlocking and powder-substrate bonding (*i.e.*, metallurgical bonding) phenomena [2]. Although substrate materials are usually metallic [3], various substrates including ceramic, polymer, and composite have also been used [5].

CSAM has been generally used to manufacture or fabricate components with rotational symmetry, including cylinder walls, tubes, flanges, and gears [6]. In addition, this technology can also be used for repairing metal manufactured parts [3,6,7]. Because the bonding mechanism of cold spray is not reliant on applying high heat or laser energy sources to melt powders, CSAM has some unique advantages over other metal powder cold spray technologies, including scalability to large product sizes, short production times, and increased equipment flexibility [3]. In addition, owing to low-operation temperature of CSAM, there is minimal heat diffusion onto the workpiece, and no phase change. As such, CSAM is promising for the rapid deposition of oxygen-sensitive materials [8]. Herein, the design of the supersonic nozzle is crucial to accelerate the micro-scale particles to desired velocities to increase the efficacy of the CS coating process since the resolution and shape of the spray spot size are highly dependent on the nozzle exit geometry [9]. Currently, CS particle deposition process mainly relies on axisymmetric nozzles as the gas flow profile has been well understood for decades. However, the particle distribution jet from an axisymmetric nozzle is quasi-Gaussian [10,11] and deposition efficiency decreases with distance from the center of the powder jet [9–12], the resulting deposition layer forms a triangle shape, with multiple side-by-side layers creating a peak-and-valley surface morphology, which limits the CSAM for many applications

---

* Corresponding author: mbgjun@purdue.edu

Recently, rectangular nozzles have promised a potential solution to the latter surface morphology problems of traditional axisymmetric nozzles by changing the powder distribution profile. Alkhimov et al. showed that rectangular nozzles are convenient for depositing relatively large particle tracks [13]. Shuo Yin et al. [14] reported that rectangular nozzles provide a larger average particle velocity compared to elliptical nozzles of similar dimensions and width to length (W/L) ratios. It was also shown that decreasing the W/L ratio does provide a weaker bow shock, although very small ratios (≤ 0.2) drastically reduce particle velocity. Studies on CS research have shown that the bow shock generated from supersonic gas flow impinging on a flat plate reduces particle impact velocity [15,16]. Varadaraajan and Mohanty [17] further optimized cold spray nozzles with rectangular cross-sections by investigating design factors such as injection angle, expansion ratio (*i.e.*, ratio of the areas of nozzle exit to throat), and nozzle traverse speed. It was found that nozzles with slightly over-expanded flows seen in simulations produced the highest simulated particle velocities compared to under-expanded flow. Of these nozzles, the nozzle with the smaller exit area (that still had an over-expanded flow) produced better deposition results, although simulations showing that the nozzles with larger exit areas producing higher particle velocity. Despite great promises, further investigation is needed to better understand the cold spray particle deposition process conducted by a rectangular nozzle in order to characterize particle deposition quality and resolution.

In the present study, we attempt to address this need by investigating micro-scale particles' flow behavior in a rectangular cold spray nozzle under different CS operating conditions. First, we utilize three-dimensional two-phase (*i.e.*, discrete phase) flow numerical modeling to characterize the particle acceleration inside and outside of the rectangular nozzle. Next, numerical modeling results are justified using a dual disc anemometer setup. Lastly, we use the rectangular nozzle in cold spray coating experiments by adopting the operational parameters from numerical modeling outputs. We also compare the resultant CS coatings achieved by the rectangular nozzle against an axisymmetric counterpart nozzle. The main key research contribution of this study is to employ three-dimensional discrete-phase modeling under supersonic flow conditions to characterize cold spray particle deposition using a rectangular nozzle and present an affordable measurement method of dual disc anemometer for capturing particles impact velocity in the cold spraying process.

2. MATERIALS

Figures 1(a)-(b) show the morphology and size distribution of the copper (Cu) feedstock material used in the cold spray (CS) coating experiments. The particles are in spherical shape having a size range of 5-44 μm, and the median particle diameter (D_{50}) is $\cong$ 36 μm. Acrylonitrile butadiene styrene (ABS) polymer plate was (ePlastics, USA) used as the substrate. CS deposition was carried out using a low-pressure CS system (Rus Sonic Technology, Inc.). Air was used as the driving gas in the
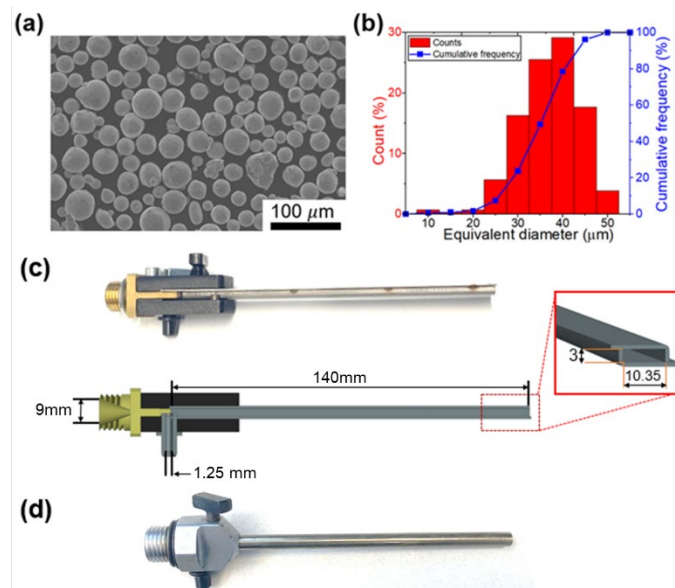

FIGURE 1: (a) CU PARTICLE MORPHOLOGY, **(b)** PARTICLE SIZE DISTRIBUTION OF THE CU PARTICLES; **(c)** SQUARE NOZZLE, **(d)** AXISYMMETRIC NOZZLE USED IN THE CS EXPERIMENTS.

experiments. The nozzles are used in the experiments are also presented in Figures 1(c)-(d). The spray nozzle was mounted on a 6-axis robot arm to precisely control the particle deposition process. The spray distance and the nozzle speed were set to 30 mm, and 50 mm/s, respectively. The microstructure of the as-cold sprayed specimens was investigated by scanning electron microscopy (SEM).

3. NUMERICAL MODELING AND THEORY

In order to properly simulate the gas and powder flow within the nozzle, a proper domain needs to be set up. This was done using ANSYS® Fluent 19.2. As shown in Figure 2, the internal geometry of the rectangular nozzle in Figure 1c was translated to a 3D model, with inlets at the start of the nozzle's converging section as well as the powder injection port. The powder injection port was set at atmospheric pressure with a powder feed rate of 1.5×10^{-4} kg.s^{-1}, and initial powder velocity of 1 m.s^{-1}. The pressure inlet boundary condition was applied to the converging section and set to 0.5-0.7 MPa above atmospheric pressure at room temperature.

At the other end of the nozzle, a 40 mm cylinder is placed at the end of the nozzle exit as the substrate, with 5mm of the cylinder protruding towards the nozzle entrance from the exit plane. With this, a rectangular cut out is placed around the nozzle exit to simulate nozzle thickness. A large section of the surface of the cylinder was set to atmospheric pressure as an inlet to improve convergence, whereas a small 5 mm-wide section around the circumference of the cylinder was set as an outlet. This section is the closest to the impingement wall at the end of the cylinder, which was set to trap the particles upon contact. As shown in Figure 2, an inflation meshing was used at the nozzle

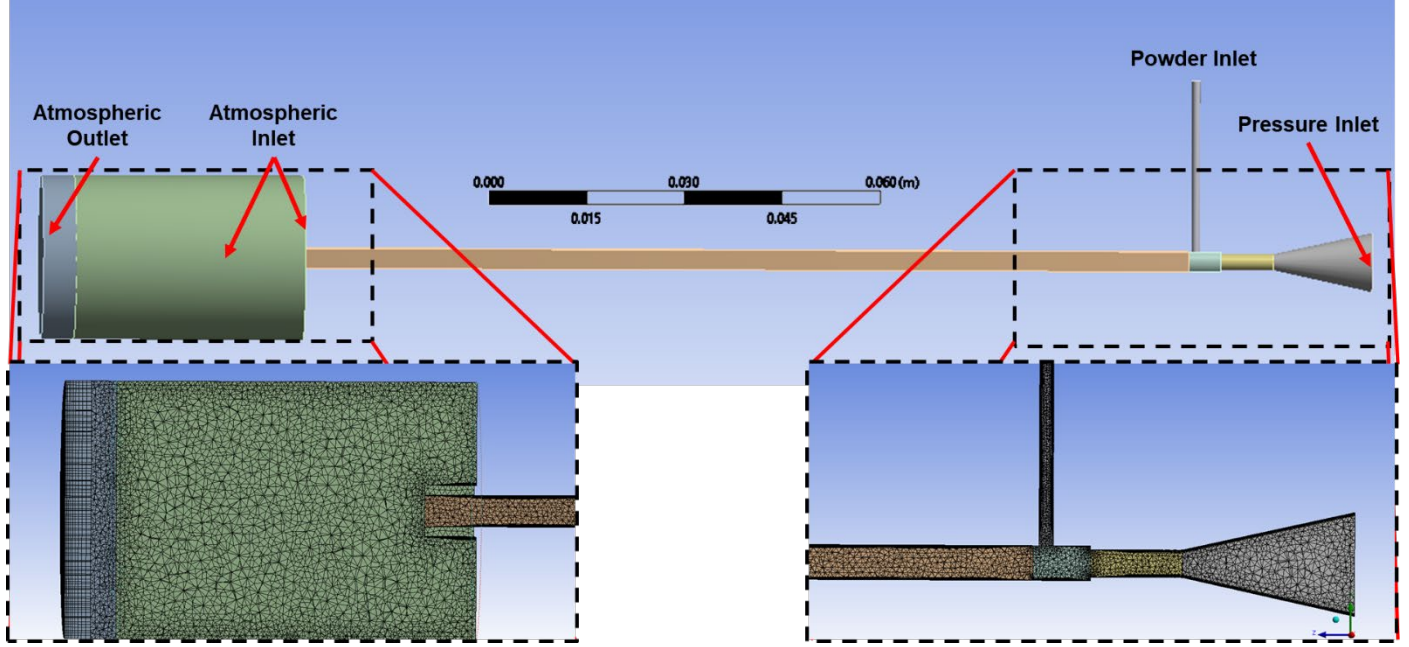and impingement walls to better capture the boundary layer effects.

FIGURE 2: COMPUTATIONAL DOMAIN AND BOUNDARY CONDITIONS, WITH MESHING CROSS SECTIONS.

To accurately represent the particle distribution as stated in Section 2, the Rosin-Rammler particle distribution was considered [18]. In here, according to the experimental particle distribution data given in Figures 1(a)-(b), the maximum powder diameter was set to 44 μm, the minimum powder diameter was set to 5 μm, and the average diameter was set to 35 μm (*i.e.*,s $\approx D_{50}$ value). The Rosin-Rammler distribution equation is as follows:

$$F_d = \exp\left(-\left(\frac{d}{\bar{d}}\right)^n\right) \quad (1)$$

where F_d is the mass fraction of the particles greater than a given particle diameter d, $\bar{d}$ is the average particle diameter, and n is the particle spread parameter set to 3.5. The number of diameter values generated in the simulation between the minimum and maximum was set to 10.

Due to the high variation in temperature, pressure, velocity, and density of CD nozzle flow, continuity, momentum, heat, and turbulence need to be considered. As such, 3D compressible flow equations are used, with gas density changing in accordance with the ideal gas law ($PV = \rho RT$), where the molar mass of air gas is 28.966 g.mol^{-1}. As the flow is compressible, the Continuity and Navier-Stokes equations used in CFD are as follows [19]:

$$\frac{\partial \rho}{\partial t} + \frac{\partial(\rho u)}{\partial x} + \frac{\partial(\rho v)}{\partial y} + \frac{\partial(\rho w)}{\partial z} = 0 \quad (2)$$

$$\rho F_x - \frac{\partial P}{\partial x} + \mu\left(\frac{\partial^2 u}{\partial x^2} + \frac{\partial^2 u}{\partial y^2} + \frac{\partial^2 u}{\partial z^2}\right) +$$
$$\frac{1}{3}\mu\frac{\partial}{\partial x}\left(\frac{\partial u}{\partial x} + \frac{\partial v}{\partial y} + \frac{\partial w}{\partial z}\right) = \rho\frac{Du}{Dt} \quad (3)$$

$$\rho F_y - \frac{\partial P}{\partial y} + \mu\left(\frac{\partial^2 v}{\partial x^2} + \frac{\partial^2 v}{\partial y^2} + \frac{\partial^2 v}{\partial z^2}\right) +$$
$$\frac{1}{3}\mu\frac{\partial}{\partial y}\left(\frac{\partial u}{\partial x} + \frac{\partial v}{\partial y} + \frac{\partial w}{\partial z}\right) = \rho\frac{Dv}{Dt} \quad (4)$$

$$\rho F_z - \frac{\partial P}{\partial z} + \mu\left(\frac{\partial^2 w}{\partial x^2} + \frac{\partial^2 w}{\partial y^2} + \frac{\partial^2 w}{\partial z^2}\right) +$$
$$\frac{1}{3}\mu\frac{\partial}{\partial z}\left(\frac{\partial u}{\partial x} + \frac{\partial v}{\partial y} + \frac{\partial w}{\partial z}\right) = \rho\frac{Dw}{Dt} \quad (5)$$

where $\frac{D}{Dt} = \frac{\partial}{\partial t} + u\frac{\partial}{\partial x} + v\frac{\partial}{\partial y} + w\frac{\partial}{\partial z}$ is the material derivative with respect to time t and velocity components $u, v,$ and w (m.s^{-1}) for coordinate directions $x, y,$ and z (m), respectively. F_i is the force component (N) in the ith direction, and P is the fluid's pressure, where gauge is set to 0 Pa and atmospheric is considered 101325 Pa. μ is the viscosity of air at (1.789×10^{-5} kg. (ms)$^{-1}$), and ρ is the gas density (kg.m^{-3}) found through the ideal gas law previous stated.

In addition, the energy equation used is as follows:

$$\frac{\partial}{\partial t}(\rho C_p T) + \frac{\partial(\rho u C_p T)}{\partial x} + \frac{\partial(\rho v C_p T)}{\partial y} + \frac{\partial(\rho w C_p T)}{\partial z}$$
$$= \frac{\partial}{\partial x}\left(k_T \frac{\partial T}{\partial x}\right) + \frac{\partial}{\partial y}\left(k_T \frac{\partial T}{\partial y}\right) + \frac{\partial}{\partial z}\left(k_T \frac{\partial T}{\partial z}\right) + S \quad (6)$$

Copyright © 2022 by ASME

In this equation, T is the gas temperature (K), C_p is the specific heat of air at 1006.43 J.(kgK)$^{-1}$, and k_T is thermal conductivity for air (0.0242 W. (mK)$^{-1}$) S is denoted by any external heat source terms, which for this case is set to zero.

Turbulence was accounted for using the realizable $k - \varepsilon$ turbulence equations [19,20]:

$$\frac{\partial}{\partial t}(\rho k) + \frac{\partial}{\partial x_j}(\rho k u_j) = \frac{\partial}{\partial x_j}\left[\left(\mu + \frac{\mu_t}{\sigma_k}\right)\frac{\partial k}{\partial x_j}\right]$$
$$+ G_k + G_b - \rho\varepsilon - Y_M + S_k \qquad (7)$$

$$\frac{\partial}{\partial t}(\rho\varepsilon) + \frac{\partial}{\partial x_j}(\rho\varepsilon u_j) = \frac{\partial}{\partial x_j}\left[\left(\mu + \frac{\mu_t}{\sigma_\varepsilon}\right)\frac{\partial\varepsilon}{\partial x_j}\right]$$
$$+ \rho C_s\sqrt{2S_{ij}S_{ij}}\,\varepsilon - \rho C_2\frac{\varepsilon^2}{k + \sqrt{\nu\varepsilon}} + C_{1\varepsilon}\frac{\varepsilon}{k}C_{3\varepsilon}G_b + S_\varepsilon \qquad (8)$$

In these sets of equations, k is the turbulent kinetic energy, ε is the turbulent rate of dissipation, and $S_{ij} = \frac{1}{2}(u_{ij} + u_{ji})$ is the fluid strain rate tensor. The total viscosity, μ is defined as $\mu = \mu_t + \mu_l$, where $\mu_t = \rho C_\mu\frac{k^2}{\varepsilon}$ is the turbulent viscosity and μ_l is the fluid's laminar viscosity. $G_k = \mu_t S^2$ and G_b are the generation of turbulent energy due to mean velocity gradients and buoyancy, respectively, and Y_M is the contribution of compressibility to turbulence, defined as $Y_M = 2\rho\varepsilon\frac{k}{a^2}$ where a is the speed of sound. ν is the fluid's kinematic viscosity, defined as $\nu = \frac{\mu}{\rho}$. The constants C_2, $C_{1\varepsilon}$, σ_k, and σ_ε have values of $C_2 = 1.9$, $C_{1\varepsilon} = 1.44$, $\sigma_k = 1.0$, $\sigma_\varepsilon = 1.2$, which are standard to the model and created by Shih et al. [20]. In addition, $C_1 = \max\left[0.43, \frac{\eta}{\eta+5}\right]$ where $\eta = S\frac{k}{\varepsilon}$. The buoyancy term G_b is defined as the following for ideal gasses:

$$G_b = -g_i\frac{\mu_t}{\rho Pr_t}\frac{\partial\rho}{\partial x_i} \qquad (9)$$

where g_i is the gravitational acceleration (m.s^{-2}) in the ith direction and $Pr_t = 0.85$ is the turbulent Prandtl number for energy. Finally, C_μ is obtained by the following equation:

$$C_\mu = \frac{1}{4.04 + \sqrt{6}\cos\varphi * \frac{kU^*}{\varepsilon}}$$
$$\widetilde{\Omega}_{ij} = \overline{\Omega}_{ij} - \varepsilon_{ijk}\omega_k - 2\varepsilon_{ijk}\omega_k \qquad (10)$$

where $U^* \equiv \sqrt{S_{ij}S_{ij} + \widetilde{\Omega}_{ij}\widetilde{\Omega}_{ij}}$, the tensor $\widetilde{\Omega}_{ij} = \overline{\Omega}_{ij} - \varepsilon_{ijk}\omega_k - 2\varepsilon_{ijk}\omega_k$, with $\overline{\Omega}_{ij}$ being the mean rate-of-rotation tensor in a moving reference frame with angular velocity ω_k. ε_{ijk} is the 3D Levi-Cita symbol. The variable φ is defined as

$$\varphi = \frac{1}{3}\cos^{-1}\left[\sqrt{6}\frac{S_{ij}S_{jk}S_{ki}}{(S_{ij}S_{ij})^{\frac{3}{2}}}\right].$$

For the powder flow modeling, a Lagrangian approach (i.e., Discrete phase modeling (DPM)) was used [19]. The governing equations are as follows:

$$m_p\frac{d\overrightarrow{v_p}}{dt} = C_D\rho(\vec{v} - \overrightarrow{v_p})|\vec{v} - \overrightarrow{v_p}|\frac{A_p}{2} + \frac{\vec{g}(\rho_p - \rho)}{\rho_p} + \vec{F} \qquad (11)$$

In this equation, $m_p\,(kg)$, v_p, and ρ_p are the particle mass, velocity, and density, respectively. In addition, A_p is the particle's cross-sectional area (m^2), C_d is the particle drag coefficient, and $\vec{F}$ are any additional forces the particle experiences during travel. The two-way coupling equation used to account for the particle-gas interaction is:

$$F_p = \sum\left(\frac{18\mu C_D Re}{\rho_p d_p^2 24}(v_p - v) + F_{other}\right)\dot{m}_p\Delta t \qquad (12)$$

where d_p is the particle's diameter, F_{other} represents any other force transferring momentum to the particles, and $\dot{m}_p$ is the powder mass flow rate. In addition, Re is the flow's Reynolds Number, defined as $Re = \frac{\rho v L}{\mu}$, with L being the characteristic length or diameter of the flow, depending on whether the gas flow is moving through the CD nozzle, flowing through open air, or impinging on the surface. For ease of calculation, the particles were assumed to be spherical, allowing for the use of the spherical drag law developed by Morsi and Alexander [21]:

$$C_D = a_1 + \frac{a_2}{Re} + \frac{a_3}{Re^2} \qquad (13)$$

The constants a_1, a_2, and a_3 are all outlined in the Morsi and Alexander paper, each one varying based on the flow's Reynolds number. It is important to note that although the model was initially created under the assumption that the flow is incompressible, but has been applied for cold spray simulations in the past [22]. Another assumption can be made that accounts for high Mach number flows: $Re_p < 300,000$ and particle Mach number $M_p > 0.4$ [23].

4. JUSTIFICATION OF NUMERICAL MODELING

To justify the numerical modeling results for particles impact velocity, we utilized a dual disc anemometer setup (i.e., originally used for measuring air-blast solid particles on substrates [24]. As seen in Figures 3 (a)-(b), the dual disc setup consists of a shaft with two rotary discs having a fixed separation distance of 33 mm. While the dual disc system was rotating, the spherical Cu particles were cold sprayed through a notch on the first disc (see Figure 3a), which leads a deposition on the second disc (i.e., recording disc). The angle difference between the notch and the resultant deposition the second disc (see Figure 3a) is measured to calculate the average particle impact velocity using an equation given below [24];
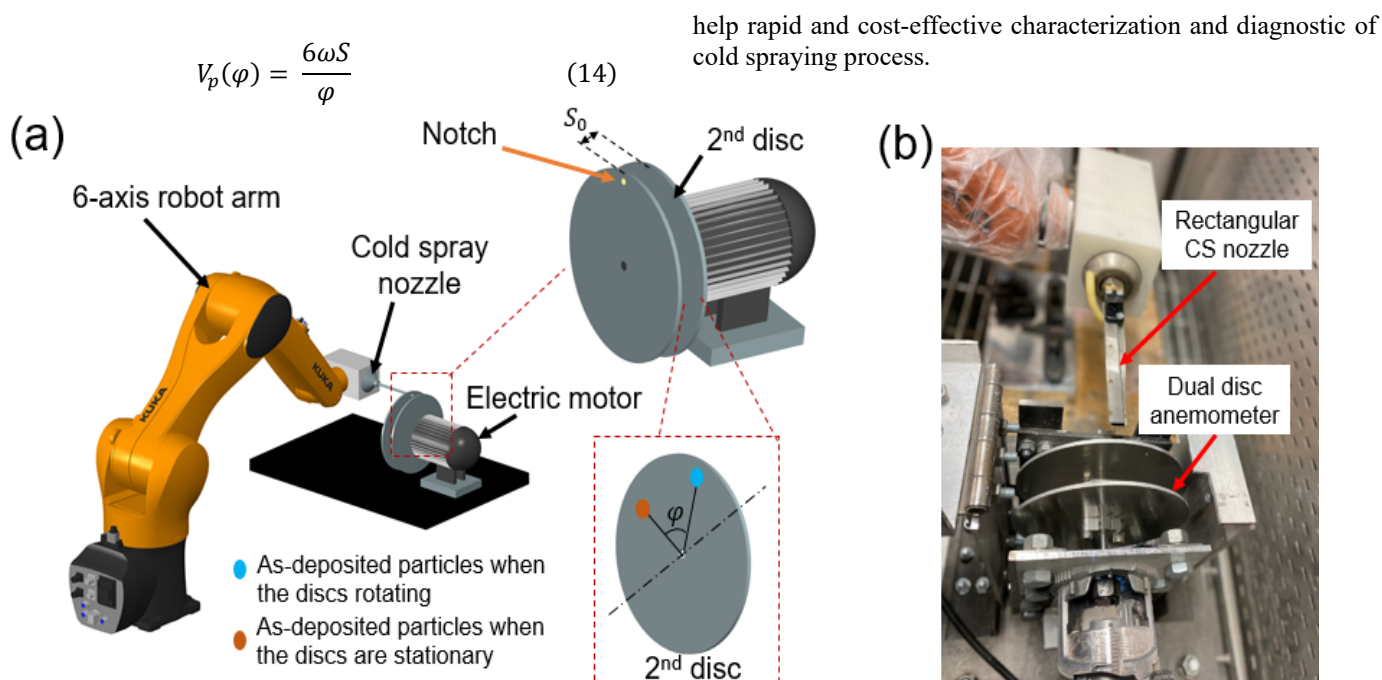
$$V_p(\varphi) = \frac{6\omega S}{\varphi} \qquad (14)$$

help rapid and cost-effective characterization and diagnostic of cold spraying process.

FIGURE 3: **(a)** SCHEMATIC OF DUAL DISC ANEOMETER INCLUDING RECORDING DISCS, **(b)** IMAGE OF THE DUAL DISC ANEMOMETER SETUP.

where V_p (m.s^{-1}) is the average particle impact velocity, S (m) is the distance between the discs, ω (rpm) is the angular velocity of the disc, and φ (degree) is the angle at which the deposits is found on the recording disc [24]. To capture the particles' impact velocity using the setup, a minimum shaft speed of 10,000 rpm was required [25]. Given that information, we measured the shaft speed as 10,630 rpm using a tachometer (Extech RPM33), and calculated the average particle impact velocity using the dual disc setup for different driving gas pressures.

Figure 4 compares the numerical modeling results with dual disc experiments at three different inlet gas pressures of 0.5, 0.6, and 0.7 MPa at room temperature. As can be seen, the results follow a similar trend with increasing driving-gas pressure. The numerical modeling results, however, predicted the particles' impact velocity larger than experimental measurements, having an error rate of < 15%, which is in a generally acceptable range for the incompressible turbulent flows [26]. The error in the numerical modeling results is likely attributed to the spatial discretization quality of the computational domain and Rosin-Rammler particle size distribution. In the present study, we used unstructured mesh (see Figure 2), which could lead to errors in calculations. In a turbulent shear flow, the boundary layer growth is critical to capture the particles' velocity in supersonic flow conditions. Given that structured mesh near to nozzle's boundary layer could help to decrease the error rate. Taken together, numerical modeling presented in this study can be pragmatically used in the characterization of cold spray particle deposition by using a rectangular nozzle configuration with a certain error. Moreover, the dual disc anemometer setup could be practically used for capturing particles impact velocity in a manner that can
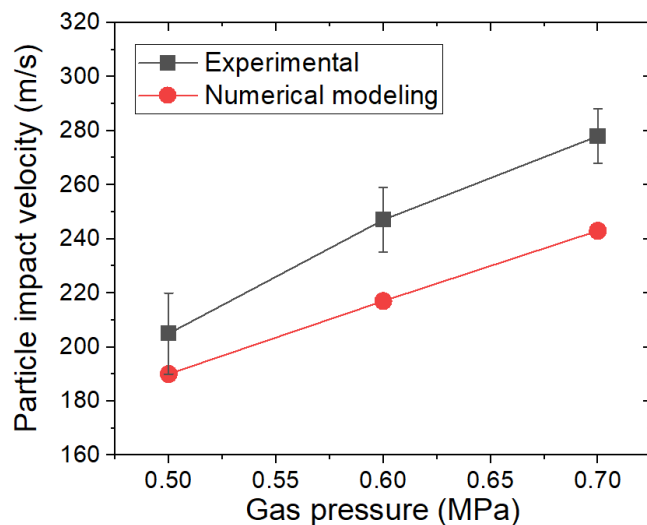

FIGURE 4: COMPARISION OF NUMERICAL MODELING AND EXPERIMENTAL DUAL DISC RESULTS FOR AVERAGE PARTICLES IMPACT VELOCITY.

5. MODELING RESULTS AND DISCUSSION

Figure 5 shows the pressure contours of the flow at different inlet gas pressures. Examination of the pressure variation within the nozzle shows that the flow separates from the nozzle walls halfway from the nozzle exit at low pressures, with that flow separation moving towards the exit as inlet pressure increases. This flow separation, as seen in Figure 5a-c, creates a shock wave pattern similar to an over-expanded jet flow, which also can exhibit mild flow separation before the nozzle exit [27].
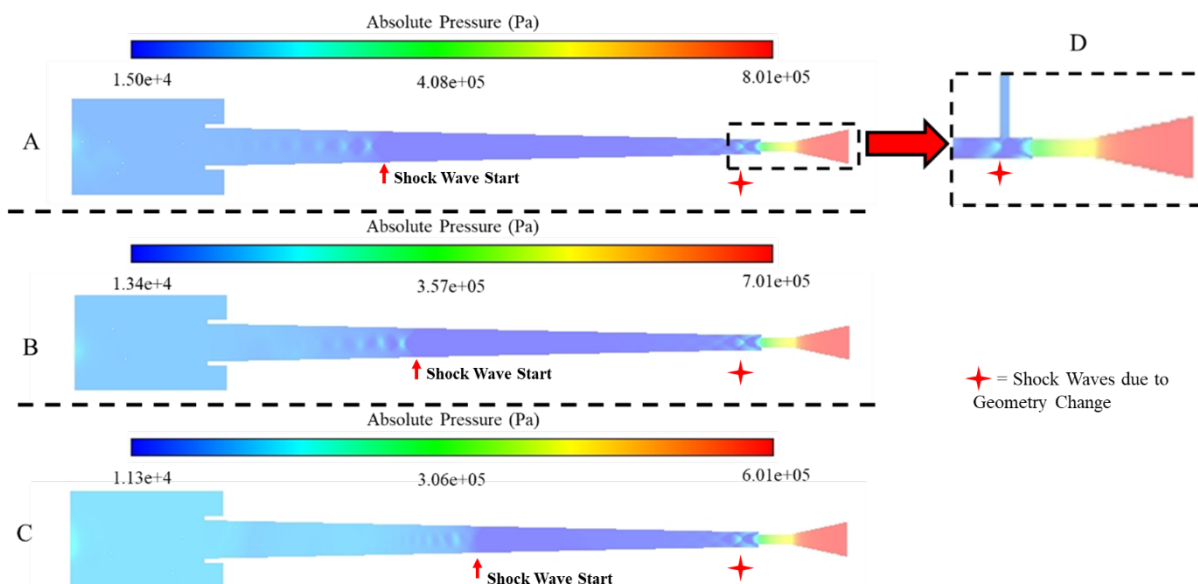
FIGURE 5: PRESSURE CONTOURS FOR **(A)** 0.7 MPA INLET PRESSURE (TOP VIEW), **(B)** 0.6 MPA INLET PRESSURE (TOP VIEW), **(C)** 0.5 MPA INLET PRESSURE (TOP VIEW), **(D)** SIDE VIEW OF THE SHOCK WAVE PATTERN FORMED AT THE TRANSITION SECTION.
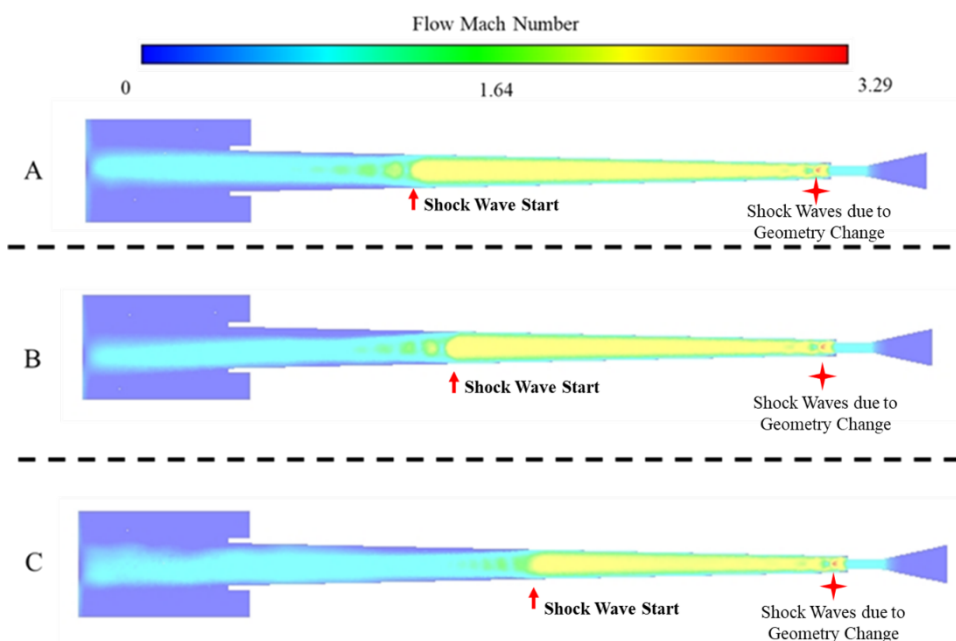

FIGURE 6: TOP VIEW MACH NUMBER CONTOURS FOR **(A)** 0.7 MPa, **(B)** 0.6 MPa, **(C)** 0.5 MPa INLET GAS PRESSURES.

Generally, low-pressure cold spray nozzles can operate using pressures up to 1.7 MPa [5]; this shows that the initial gas inlet conditions are relatively low. When referring to standard CD nozzle flow, there are cases where the pressure difference between the inlet pressure and the back pressure (in this case atmospheric pressure) is low enough to form a shock wave in the nozzle [28]. These shockwaves are typically normal to the flow, producing an abrupt change in gas velocity over the shock wave. However, because of the rectangular nozzle's geometry, normal shock waves are unable to form. Instead, flow separation forms with oblique shock waves within the nozzle. This, in turn,

ensures that the gas velocity post-separation reduces in a more gradual manner, which can be seen in Figure 6. As such, the rectangular nozzle ensures that the gas can continue to accelerate the powders as they travel further down the nozzle. In addition, it is possible that the rectangular nozzle allows for an increased operating pressure range due to the developed flow pattern.

One other interesting aspect of the rectangular nozzle is the geometry of the injection point (Figure 5d). Because this nozzle is designed to be interchangeable with a circular nozzle provided by the manufacturer, the inlet and throat are consistently circular. To reduce the drastic change from circular throat to rectangular
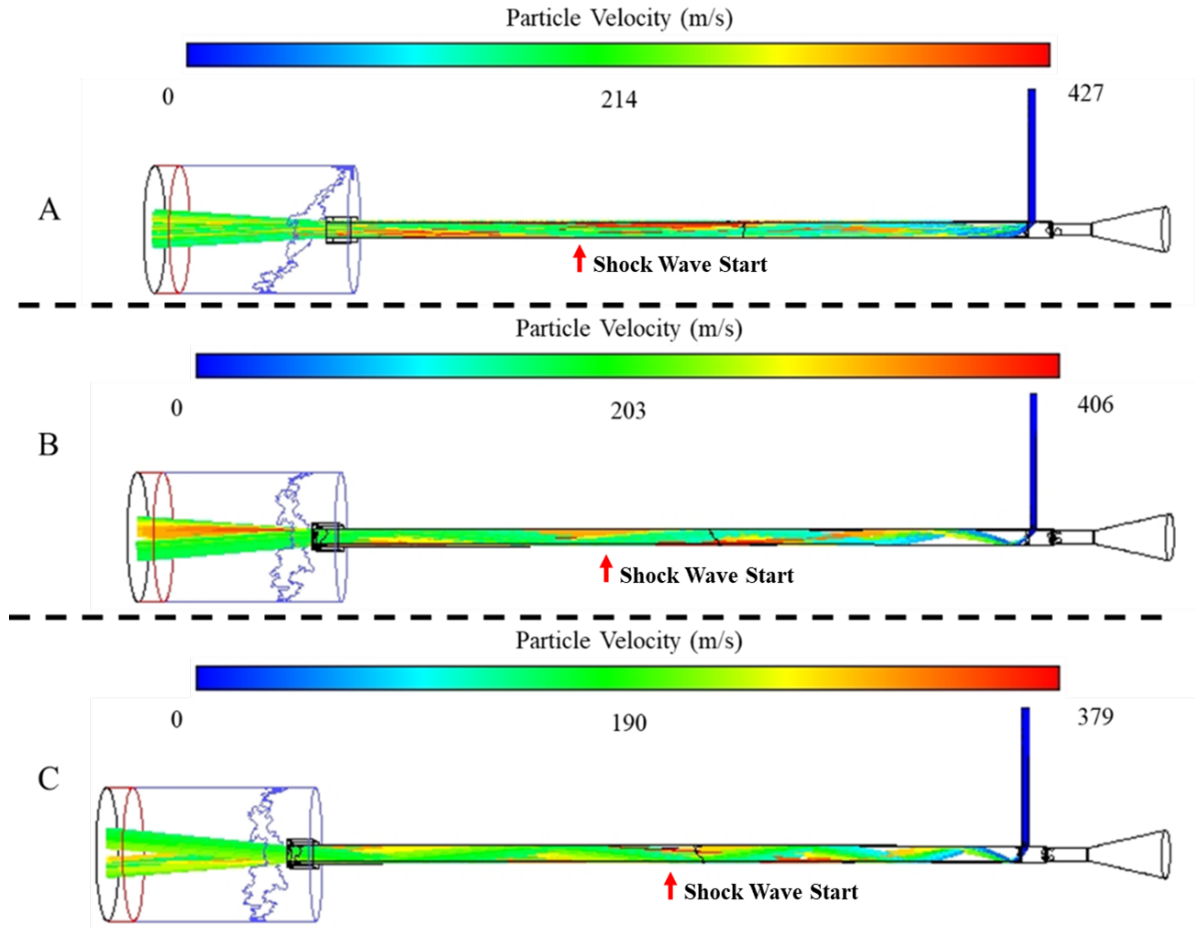
FIGURE 7: PARTICLE VELOCITY TRAJECTORIES FOR **(A)** 0.7 MPa, **(B)** 0.6 MPa, **(C)** 0.5 MPa INLET GAS PRESSURES. LOCATIONS OF CORRESPONDING SHOCK WAVES ARE SHOWN FOR COMPARISON WITH FIGURES 5 AND 6.

diverging section, a transition section is used. This transition section abruptly changes the effective diameter of the nozzle after the throat, resulting in a stationary oblique shock-wave pattern. The gas flow within this section shows the maximum gas velocity within the nozzle, as well as the lowest pressure, making it the optimal location for the powder injection port. However, as seen in Figure 5d, the inclusion of an injection port also results in the formation of another shock wave.

Despite the numerous shock wave patterns displayed in the nozzle, the particle trajectories – seen in Figure 7 – do not seem to be drastically affected by the shock-wave pattern within the nozzle. At the point of the shock waves, no reduction in powder velocity nor change in particle trajectory within the nozzle was observed. It is likely attributed to sufficient inertia and momentum of micro-scale Cu particles to overcome the oblique and normal shock waves. Indeed, other studies have shown that the shock-wave pattern formed by free-stream nozzle gas flow does not drastically affect particle velocity whereas strong shock waves such as bow shocks formed above the surface decrease particle velocity [22]. In the simulations, particles immediately are caught by the high-speed air flow, ricocheting off the nozzle walls and increasing in speed until exiting the nozzle. From there, the particles continue on their exit trajectories towards the surface, where the particle "trapped" boundary condition catches them. Although the average particle velocities shown in Figure 4 are within acceptable error (i.e., <15%) of experimental values, the range of particle velocities varies drastically from the average. For example, in the 0.7 MPa case, the highest particle velocities reached up to 427 m/s, and the lowest only achieved 126 m/s (see Figure 7a). In addition, the particle velocities seem to land in an area that is slightly wider than the nozzle profile, with a decrease in particle spreading as pressure increases. This indicates that higher gas pressures improve overall spray deposition quality as it forces particle velocity vectors to become more parallel with the nozzle direction even after exiting the nozzle. Taking into account the data from Figure 4, further improvements to the mesh (creating a more structured mesh, reducing cell size within the mesh) can improve the overall accuracy of the particle trajectories. However, even with an unstructured mesh, particle trajectories and velocities can be modeled with acceptable accuracy.

6. EXPERIMENTAL DEPOSITION ANALYSIS

Based on the numerical modeling results in Section 3, an experimental case study on polymer surface metallization using

Copyright © 2022 by ASME

different nozzle configurations (*i.e.*, axisymmetric and rectangular shape) was conducted. The cold spray operating
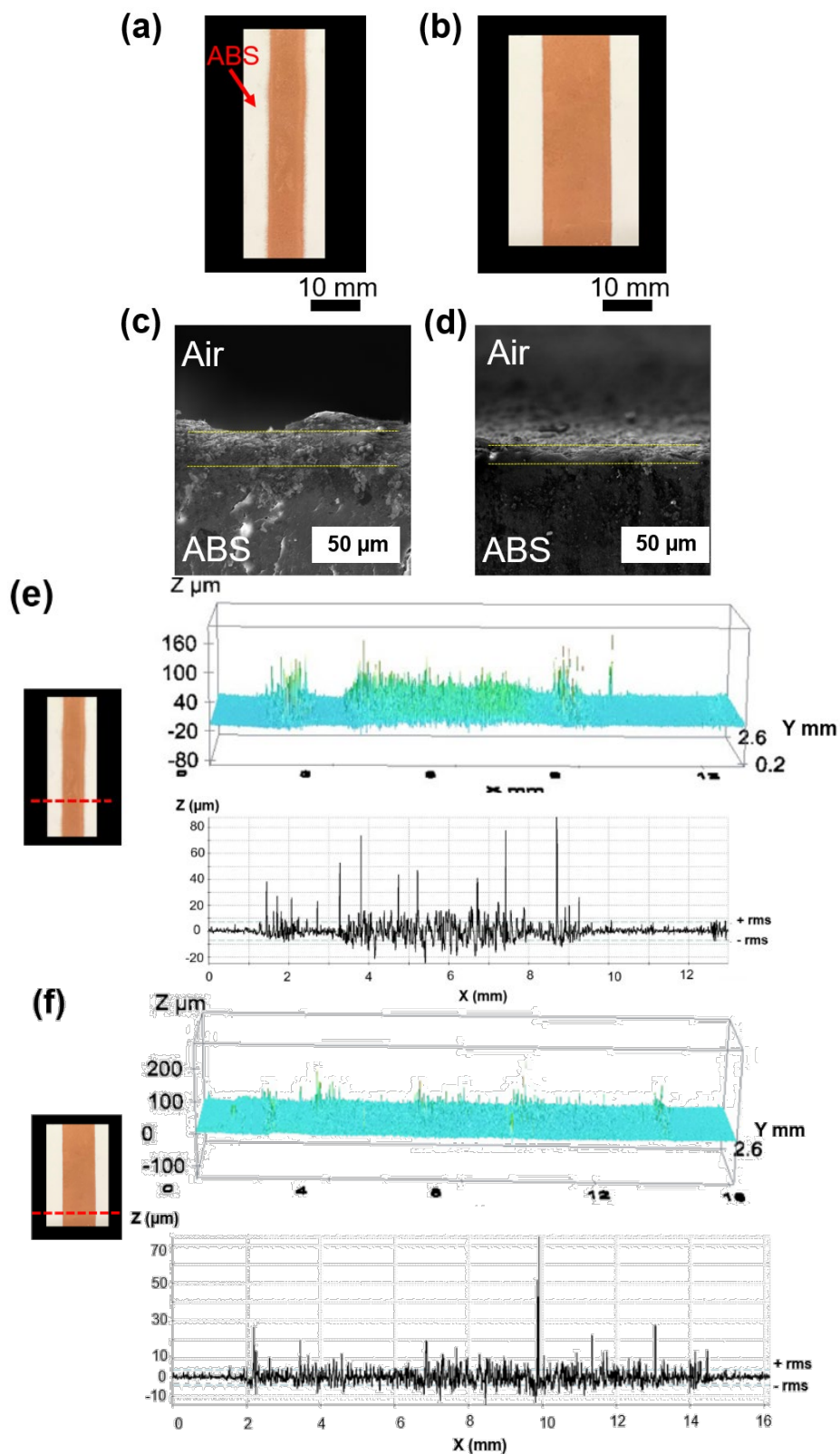
FIGURE 8: RESULTANT COLD SPRAY COATINGS USING THE **(a)** AXISYMMETRIC NOZZLE, **(b)** RECTANGULAR NOZZLE; CROSS-SECTION SEM IMAGES OF THE COATINGS; **(c)** AXISYMMETRIC NOZZLE, **(d)** RECTANGULAR NOZZLE; SURFACE TOPOGRAPGHY AND ROUGHNESS OF THE COATINGS WITH **(e)** AXISYMMETRIC NOZZLE, **(f)** RECTANGULAR NOZZLE.

parameters used in the experiments are listed in Table 1. Air was used as the driving gas and the pressure (gauge) was set to 0.7 MPa in the experiments correspondingly as the numerical results (see Figure 7a) indicated that inlet pressure of 0.7 MPa reduced particle stream dispersion. Also, numerical modeling results helped us to select the experimental operating conditions. Given that the Cu feedstock particles were sprayed on the ABS polymer substrate using both rectangular and on axisymmetric nozzle configurations under vacuum-and mask-free conditions.

TABLE 2 COLD SPRAY OPERATING PARAMETERS.

Working gas	Air
Gas inlet gauge pressure (MPa)	0.7
Gas inlet temperature (K)	400
Powder flow rate (g.s^{-1})	0.3
Nozzle transverse speed (mm.s^{-1})	50
Nozzle stand-off distance (mm)	30

Figures 8(a)-(f) show the characterization of as-cold sprayed ABS specimens. As can be seen in Figures 8 (a)-(b), the coating obtained by rectangular nozzle configuration has a more uniform Cu particle distribution having clear boundaries, which is different than the coating obtained by the axisymmetric nozzle. This can be better seen from the cross-section SEM images in Figures 8(c)-(d) showing that the coating with rectangular nozzle configuration (see Figure 8d) promises significantly uniform deposition on the polymer surface compared to the axisymmetric nozzle. Another important finding is that the particles impinge more onto/into the polymer surface when the axisymmetric nozzle is used (Figure 8c). It can be attributed to the higher impact velocity of particles, which have more kinetic energy gain to impinge the ABS surface. In our previous study on cold spray [25], we experienced higher impact velocities (*i.e.*, ≅ 15% higher) for the same Cu feedstock materials for the axisymmetric nozzle configuration. These results suggest that axisymmetric nozzles can accelerate micro-scale metal particles to higher velocities than rectangular cold spray nozzles.

Figures 8(e)-(f) show the surface morphology and roughness of the resultant cold spray coatings on ABS surface observed by using a confocal microscope (Leica DCM8). As can be seen, the coating obtained from the axisymmetric nozzle has significantly rougher topology (see Figure 8e) in particular in the middle section of the travelling path as compared to the coating with rectangular nozzle (Figure 8f). Accordingly, surface roughness measurement (see bottom panels of Figures 8(e)-(f)) indicates that the CS coating by the axisymmetric nozzle comprises severe valley formation in the middle section of the coating due to the dominated Rosin-Rammler particle distribution for axisymmetric nozzle configuration, which is undesired for additive manufacturing applications. Conversely, the rectangular nozzle ensures more uniform particle distribution on the polymer surface having clear boundaries at the edges as compared to the axisymmetric nozzle, which is such a desired

property for CSAM. The average surface roughness (S_a) values were calculated as 6.6 μm and 3.02 μm for the axisymmetric and rectangular nozzles respectively, which also proves the critically higher uniformity of the coatings obtained by rectangular nozzle configuration against the axisymmetric nozzle configuration.

Here, it is noteworthy that cold spray additive manufacturing (CSAM) on a polymer surface is challenging due to the particles deposition phenomenon. More specifically, the deposition of the first layer of Cu particles on the polymer surface is achieved by the interlocking of particles with the polymer surface due to the softer nature of the polymer against the metal substrates [29]. The upcoming layers, however, will require metallurgical bonding of particles onto previously metalized layer (*i.e.*, as-cold sprayed first layer). That means that the critical velocity to bond Cu particles onto as-metallized layer (*i.e.*, as-cold sprayed surface) should be achieved for a successful additive manufacturing (AM) process. However, rectangular nozzles lead to lower impact velocities compared to circular nozzles, which require higher driving gas pressures to achieve desired velocities. As can be seen in Figure 4, the maximum particle velocity was achieved as ≅ 290 m/s at the inlet gas pressure of 0.7 MPa, which is below the critical velocity of Cu particles required to be metallurgically bonded on the as-cold sprayed Cu layer (*i.e.*, 520- 570 m/s for the particle size of 5-30 μm [1,30,31]. Lower impact velocities than the critical velocity on the as-cold sprayed layer generally result in erosion instead of additive deposition [25,32–34]. Although the polymer surface can be successfully metallized using an inlet gas pressure of 0.7 MPa, CSAM on polymer substrate requires higher gas pressures to achieve a critical velocity range to ensure metallurgical bonding of metal particles (*e.g.*, copper) on the polymer surface without eroding the base polymer substrate.

Taken together, the rectangular nozzle configuration offers uniform particle distribution onto the polymer surface while accelerating the particles to lower velocities than the axisymmetric nozzle. The results suggest that cold spraying with rectangular nozzles is the better choice against the traditional axisymmetric nozzles for additive manufacturing applications owing to more uniform particle distribution on the substrate surface, resulting in less valley formation compared to axisymmetric counterpart nozzles.

7. CONCLUSION

In this study, cold spray particle deposition using a rectangular nozzle was investigated by numerical modeling. A three-dimensional turbulent flow modeling was utilized to study the microscale (*i.e.*, 5-44 μm) copper (Cu) particles behavior under rectangular nozzle flow conditions. A dual-disc anemometer setup was used to justify the numerical modeling by capturing the impact velocity of cold sprayed particles. An experimental case study on cold spray-based polymer metallization was conducted using both rectangular and axisymmetric nozzles. The following conclusion can be drawn from the present study:

- Numerical modeling results have a similar trend with the experimental dual disc measurements, having an error rate of < 15%.
- Although the dual disc setup is not as precise as laser-based particle velocity measurement systems (*e.g.*, PIV and LDV), it is a simple and cost-effective system, which has the potential as a measurement/diagnostic tool for cold spray applications.
- Cold particle deposition with rectangular nozzle leads to more uniform particle distribution on the ABS polymer surface compared to the traditional axisymmetric nozzle, having clear coating boundaries.
- Rectangular nozzle is the better choice for cold spray additive manufacturing (CSAM) applications on polymer surfaces owing to its more uniform particle distribution with minimized valley/peak formation compared to axisymmetric nozzles.
- The use of a rectangular nozzle leads to a lower particle impact velocity compared to an axisymmetric nozzle, which should be carefully considered to achieve desired critical velocities for CSAM using rectangular nozzles.
- The numerical simulations, experimental justification, and case study reveal that a cold spray setup having the rectangular nozzle configuration could lead to better performance for polymer metallization applications in a rapid and high-throughput manner.
- Although microscale film metallization on polymer surface was achieved in a rapid and uniform manner by using a rectangular nozzle, layer by layer additive manufacturing on as-cold sprayed layer remains challenging due to a need for higher impact velocities to ensure metallurgical bonding between the upcoming particles and as-deposited particles.
- For future work, the authors will focus on optimization of the cold spray process parameters (*e.g.*, gas pressure and temperature, nozzle speed, spray distance, and particle flow rate) using rectangular nozzle configuration for thick metal film fabrication on polymer substrates. In addition, further comparison between the rectangular and axisymmetric nozzles will be performed both in simulations and experiments.

8. REFERENCES

[1] Klassen, T., Gärtner, F., Schmidt, T., Kliemann, J. O., Onizawa, K., Donner, K. R., Gutzmann, H., Binder, K., and Kreye, H., 2010, "Basic Principles and Application Potentials of Cold Gas Spraying," *Materialwissenschaft Und Werkstofftechnik*, John Wiley & Sons, Ltd, pp. 575–584.

[2] Raoelison, R. N., Xie, Y., Sapanathan, T., Planche, M. P., Kromer, R., Costil, S., and Langlade, C., 2018, "Cold Gas Dynamic Spray Technology: A Comprehensive Review of Processing Conditions for Various Technological Developments till to Date," Addit. Manuf., **19**, pp. 134–159.

[3] Yin, S., Cavaliere, P., Aldwell, B., Jenkins, R., Liao, H., Li, W., and Lupoi, R., 2018, "Cold Spray Additive Manufacturing and Repair: Fundamentals and Applications," Addit. Manuf., **21**, pp. 628–650.

[4] Irissou, E., Legoux, J. G., Ryabinin, A. N., Jodoin, B., and Moreau, C., 2008, "Review on Cold Spray Process and Technology: Part I - Intellectual Property," J. Therm. Spray Technol., **17**(4), pp. 495–516.

[5] Moridi, A., Hassani-Gangaraj, S. M., Guagliano, M., and Dao, M., 2014, "Cold Spray Coating: Review of Material Systems and Future Perspectives," Surf. Eng., **30**(6), pp. 369–395.

[6] Champagne, V., and Helfritch, D., 2016, "The Unique Abilities of Cold Spray Deposition FULL CRITICAL REVIEW The Unique Abilities of Cold Spray Deposition," Int. Mater. Rev., **61**.

[7] Champagne, V. K., 2007, "Repair of Magnesium Components by Cold Spray Techniques," Cold Spray Mater. Depos. Process Fundam. Appl., pp. 327–352.

[8] Pathak, S., and Saha, G. C., 2017, "Development of Sustainable Cold Spray Coatings and 3D Additive Manufacturing Components for Repair/Manufacturing Applications: A Critical Review," Coatings, **7**(8), p. 122.

[9] Papyrin, A., 2007, *The Development of the Cold Spray Process*, Woodhead Publishing Limited.

[10] Sova, A., Grigoriev, S., Okunkova, A., and Smurov, I., 2013, "Potential of Cold Gas Dynamic Spray as Additive Manufacturing Technology," Int. J. Adv. Manuf. Technol., **69**(9–12), pp. 2269–2278.

[11] Pattison J, Celotto S, Morgan R, O. W., 2005, "Cold Spray Nozzle Design and Performance Evaluation Using Particle Image Velocimetry," *Proceedings of International Thermal Spray Conference,* Basel, Switzerland.

[12] Gilmore, D. L., Dykhuizen, R. C., Neiser, R. A., Roemer, T. J., and Smith, M. F., "Particle Velocity and Deposition Efficiency in the Cold Spray Process."

[13] Alkhimov, A. P., Kosarev, V. F., and Klinkov, S. V., 2001, "The Features of Cold Spray Nozzle Design," J. Therm. Spray Technol. 2001 102, **10**(2), pp. 375–381.

[14] Yin, S., Wang, X. fang, and Li, W. ya, 2011, "Computational Analysis of the Effect of Nozzle Cross-Section Shape on Gas Flow and Particle Acceleration in Cold Spraying," Surf. Coatings Technol., **205**(8–9), pp. 2970–2977.

[15] Akin, S., Wu, P., Tsai, J. T., Nath, C., Chen, J., and Jun, M. B. G., 2021, "A Study on Droplets Dispersion and Deposition Characteristics under Supersonic Spray Flow for Nanomaterial Coating Applications," Surf. Coatings Technol., **426**, p. 127788.

[16] Lee, M. W., Park, J. J., Kim, D. Y., Yoon, S. S., Kim, H. Y., Kim, D. H., James, S. C., Chandra, S., Coyle, T., Ryu, J. H., Yoon, W. H., and Park, D. S., 2011, "Optimization of Supersonic Nozzle Flow for Titanium Dioxide Thin-Film Coating by Aerosol Deposition," J. Aerosol Sci.,

42(11), pp. 771–780.

[17] Varadaraajan, V., and Mohanty, P., 2017, "Design and Optimization of Rectangular Cold Spray Nozzle: Radial Injection Angle, Expansion Ratio and Traverse Speed," Surf. Coatings Technol., **316**, pp. 246–254.

[18] Rosin, P., and Rammler, E., 1933, "The Laws Governing the Fineness of Powdered Coal," J. Inst. Fuel, **7**, pp. 29–36.

[19] Fluent Thoery Guide, 2013, "Ansys Fluent Theory Guide," ANSYS Inc., USA, **15317**(November), pp. 724–746.

[20] Shih, T.-H., Liou, W. W., Shabbir, A., Yang, Z., and Zhu, J., 1995, "A NEW K-ε EDDY VISCOSITY MODEL FOR HIGH REYNOLDS NUMBER TURBULENT FLOWS," Compuers Fluids, **24**(3), pp. 227–238.

[21] Morsi, S. A., and Alexander, A. J., 1972, "An Investigation of Particle Trajectories in Two-Phase Flow Systems," J. Fluid Mech., **55**(2), pp. 193–208.

[22] Jen, T. C., Li, L., Cui, W., Chen, Q., and Zhang, X., 2005, "Numerical Investigations on Cold Gas Dynamic Spray Process with Nano- and Microsize Particles," Int. J. Heat Mass Transf., **48**(21–22), pp. 4384–4396.

[23] Clift, R., Grace, J., and Weber, M., 2005, "Bubbles, Drops, and Particles."

[24] Haghbin, N., Khakpour, A., Schwartzentruber, J., and Papini, M., 2019, "Measurement of Abrasive Particle Velocity and Size Distribution in High Pressure Abrasive Slurry and Water Micro-Jets Using a Modified Dual Disc Anemometer," J. Mater. Process. Technol., **263**, pp. 164–175.

[25] Tsai, J. T., Akin, S., Zhou, F., Bahr, D. F., and Jun, M. B. G., 2021, "Establishing a Cold Spray Particle Deposition Window on Polymer Substrate," J. Therm. Spray Technol., **30**(4), pp. 1069–1080.

[26] Varga, S., Oliveira, A. C., Ma, X., Omer, S. A., Zhang, W., and Riffat, S. B., 2011, "Comparison of CFD and Experimental Performance Results of a Variable Area Ratio Steam Ejector," Int. J. Low-Carbon Technol., **6**(2), pp. 119–124.

[27] Li, W. Y., Liao, H., Douchy, G., and Coddet, C., 2007, "Optimal Design of a Cold Spray Nozzle by Numerical Analysis of Particle Velocity and Experimental Validation with 316L Stainless Steel Powder," Mater. Des., **28**(7), pp. 2129–2137.

[28] Zucrow, M. J., and Hoffman, J. D., 1976, *Gas Dynamics*, John Wiley and Sons Inc., New York.

[29] Melentiev, R., Yu, N., and Lubineau, G., 2021, "Polymer Metallization via Cold Spray Additive Manufacturing: A Review of Process Control, Coating Qualities, and Prospective Applications," Addit. Manuf., **48**, p. 102459.

[30] Hussain, T., McCartney, D. G., Shipway, P. H., and Zhang, D., 2009, "Bonding Mechanisms in Cold Spraying: The Contributions of Metallurgical and Mechanical Components," J. Therm. Spray Technol., **18**(3), pp. 364–379.

[31] Raletz, F., Vardelle, M., and Ezo'o, G., 2006, "Critical Particle Velocity under Cold Spray Conditions," Surf. Coatings Technol., **201**(5), pp. 1942–1947.

[32] Che, H., Liberati, A. C., Chu, X., Chen, M., Nobari, A., Vo, P., and Yue, S., 2021, "Metallization of Polymers by Cold Spraying with Low Melting Point Powders," Surf. Coatings Technol., **418**, p. 127229.

[33] Akin, S., Tsai, J. T., Park, M. S., Jeong, Y. H., and Jun, M. B. G., 2020, "Fabrication of Electrically Conductive Patterns on Acrylonitrile-Butadiene-Styrene Polymer Using Low-Pressure Cold Spray and Electroless Plating," J. Micro Nano-Manufacturing, **8**(4).

[34] Tsai, J.-T., Akin, S., Zhou, F., Park, M. S., Bahr, D. F., and Jun, M. B.-G., 2022, "Electrically Conductive Metallized Polymers by Cold Spray and Co-Electroless Deposition," ASME Open J. Eng., **1**.

DECLARATION OF COMPETING INTEREST

The authors declare no competing interests.

AUTHOR CONTRIBUTIONS

Ted Gabor: concept, formal analysis, design, simulations, experiments, characterization, data curation, writing original draft, ***Semih Akin***: concept, formal analysis, design, experiments, data curation, writing original draft, ***Jung-Ting Tsai***: experiments, characterization, ***Seunghwan Jo:*** experiments, characterization, ***Feraas Al-Najjar:*** experiments, ***Martin Byung-Guk Jun:*** concept, supervision, review & editing. All authors commented on the paper.